



## Avanços em Ciência e Engenharia de Materiais

[+ Journal Menu](#)[PDF](#)[Article Sections](#)**Artigo de pesquisa | Acesso livre**Volume 2020 | Artigo ID 7109382 | <https://doi.org/10.1155/2020/7109382>[Show citation](#)

# Fire Resistance of Composite Beams with Restrained Superposed Slabs

Junli Lyu  ,<sup>1,2</sup> Qichao Chen,<sup>1</sup> Huizhong Xue,<sup>1,2</sup> Yongyuan Cai,<sup>1</sup> Jingjing Lyu,<sup>1</sup> and Shengnan Zhou<sup>1</sup>[Show more](#)**Academic Editor:** María Criado**Published:** 10 Jul 2020

## Abstract

To investigate the fire resistance of composite beams with restrained superposed slabs, three specimens were tested under uniformly distributed loads in a furnace. The effects of the thickness of the postcast top layer in superposed slabs and the spacing of shear studs on the structural behaviours of composite beams under fire were further examined. During the tests, the temperature distributions of the superposed slabs and steel beams as well as the displacements at their key positions were recorded and analysed. It was found that the temperature of the concrete superposed slabs decreased long their heights from the bottom. The most drastic change of the temperature along the slab cross section was found in the region with a distance of 40 mm to the slab bottom. The concrete superposed slabs could impose restraints to the steel beams due to their incompatible deformations. Cracks were developed on the top surfaces of the specimens and the superposing interfaces between the precast slabs and postcast top layers were not broken. Through the comparisons of different specimens, the spacing of shear studs could have a significant effect on the fire resistance of composite beams, especially for their deformation recovery capacities. In contrast, the effect of the thickness of the postcast top layers was negligible. ABAQUS was employed to simulate the temperature fields and deformation behaviours of composite beam specimens based on a sequenced thermomechanical coupling analysis. The numerical results agreed well with the experiment data, which validated the developed numerical model.

## 1. Introdução

## Avanços em Ciência e Engenharia de Materiais

+ Journal Menu

PDF



### Article Sections

rossem fornecidas restrições horizontais adequadas para as vigas mistas. Mirza e Uy [ 5 ] estudaram as influências dos conectores de cisalhamento na resistência ao fogo de vigas mistas por meio de estudos numéricos utilizando o software de elementos finitos ABAQUS. Verificou-se que os conectores de cisalhamento afetaram ligeiramente o desempenho estrutural das vigas mistas com chapa de aço perfilada, enquanto as vigas mistas com lajes planas podem falhar devido à ruptura dos conectores de cisalhamento. No entanto, outros pesquisadores [ 4 – 7 ] mostrou que a chapa de aço ainda pode se desprender da viga de aço em testes de incêndio, uma vez que os pinos de cisalhamento foram instalados corretamente, levando a uma redução da capacidade de carga e de deformação. Além disso, uma maior resistência ao fogo poderia ser alcançada se as vigas mistas com chapa de aço perfilada fossem restringidas longitudinalmente. Da mesma forma, a análise teórica [ 8 ] também mostrou que as restrições nas extremidades das vigas também podem melhorar a resistência ao fogo de vigas mistas com lajes planas.

A influência de diferentes tipos de chapas de aço perfiladas na resistência ao fogo de vigas mistas também foi examinada [ 9 ] e os resultados mostraram que a contribuição da chapa de aço perfilada pode ser desprezada para o cálculo da resistência à flexão. Lyu et al. [ 10 - 13 ] realizaram testes de incêndio em vigas mistas com lajes planas e descobriram que a viga de aço e a laje de concreto poderiam se comportar em conjunto com um melhor desempenho estrutural se uma quantidade suficiente de conectores de cisalhamento fossem dispostos. Além disso, a ação catenária não foi observada, pois apenas pequenas deformações das vigas mistas foram desenvolvidas nos ensaios de incêndio. A partir dos estudos existentes, mostra-se que as vigas mistas com diferentes tipos de lajes comportam-se de forma distinta nos ensaios de incêndio e as vigas mistas restringidas apresentam uma melhor resistência ao fogo. Além disso, a análise numérica usando software de elementos finitos é uma abordagem eficaz para investigar o comportamento estrutural de vigas mistas sob fogo.

As vigas mistas com lajes sobrepostas são um novo tipo de elemento estrutural e consistem em vigas de aço e lajes de concreto sobrepostas. As lajes sobrepostas são diferentes das tradicionais lajes de concreto, pois são compostas por uma camada base de lajes pré-moldadas e uma camada superior de concreto pós-moldado. Neste artigo, o comportamento estrutural de três vigas mistas com lajes sobrepostas restritas ao fogo são examinados através de estudos experimentais e simulações numéricas.

## 2. Programa Experimental

### 2.1. Projeto de Amostra

Três corpos de prova de vigas mistas com lajes sobrepostas (SCB-1–3), consistindo de uma viga de aço, lajes sobrepostas de concreto e pinos de cisalhamento, foram projetados e fabricados de acordo com as normas de engenharia relevantes. O comprimento total das vigas mistas foi de 4.300 mm e a largura dos banzos foi de 1.625 mm. As lajes sobrepostas de concreto foram compostas por uma camada base pré-moldada de 60 mm de espessura e uma camada superior pós-moldada. O grau nominal de concreto para

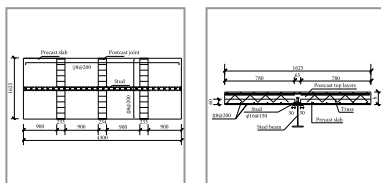
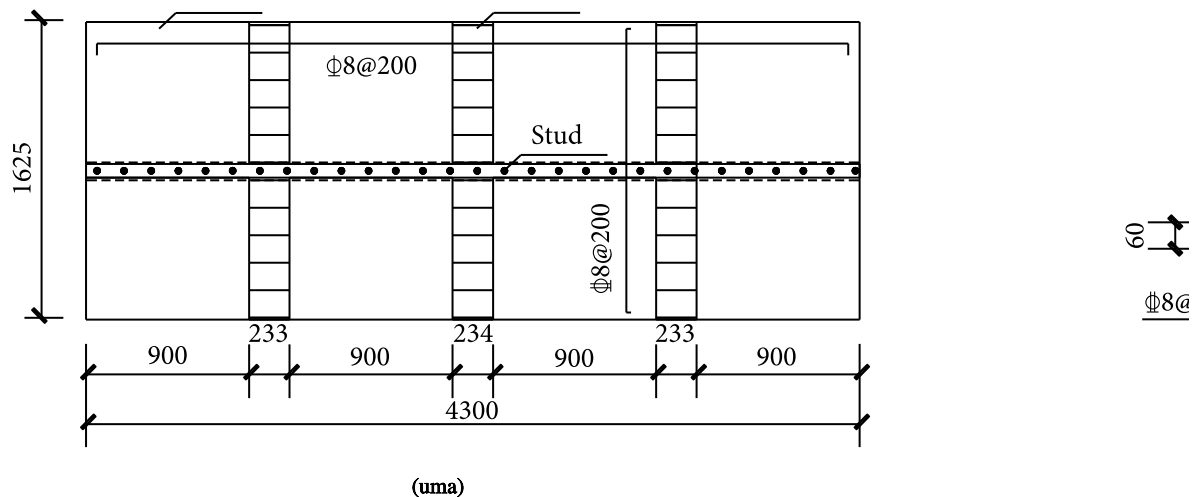
## Avanços em Ciência e Engenharia de Materiais

+ Journal Menu

PDF



Article Sections



(uma)

(b)

**figura 1**

Detalhes da amostra: (a) vista em planta e (b) vista em corte (unidade: mm).

**tabela 1**

Parâmetros variados dos corpos de prova testados (unidade: mm).

## 2.2. Propriedades do Material

Atendendo aos requisitos construtivos, as lajes sobrepostas foram fabricadas em duas etapas. Na primeira etapa, as lajes pré-moldadas foram fabricadas e colocadas no local, após o que o concreto da camada superior do pós-moldado foi derramado. Junto com a fabricação dos corpos de prova, três conjuntos de cubos de concreto padrão com dimensão nominal de 150 mm foram produzidos e curados nas mesmas

## Avanços em Ciência e Engenharia de Materiais

+ Journal Menu

PDF



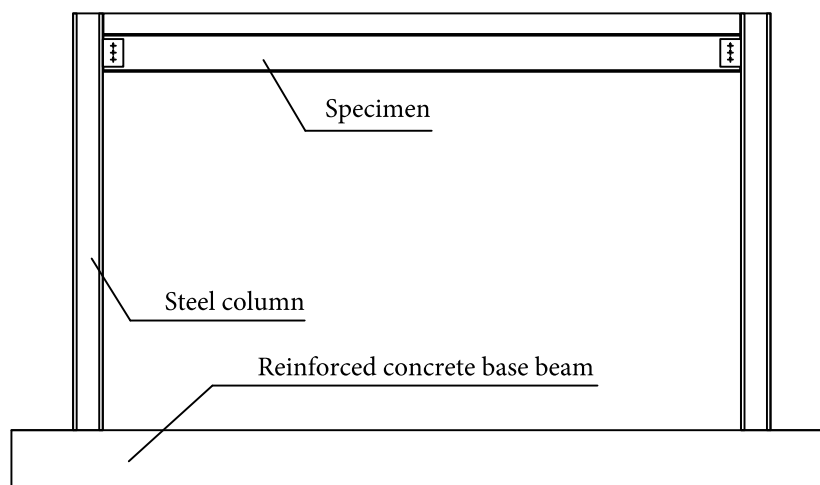
Article Sections

### Tabela 3

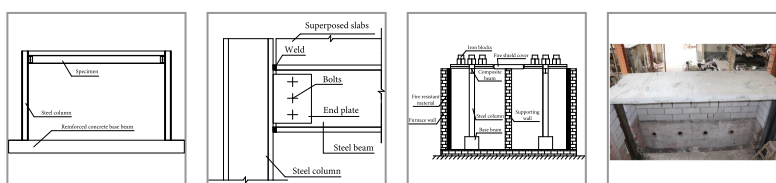
Propriedades do material do aço não queimado.

### 2.3. Condições de fronteira

Os testes foram realizados no Laboratório de Incêndio da Universidade Shandong Jianzhu. O forno foi modificado com base nos requisitos do teste e permitiu que dois espécimes fossem testados ao mesmo tempo. Para contenção dos corpos de prova, uma viga de base de concreto armado e dois pilares de aço (Figura 2(a)) foram fabricados e montados. Durante os testes de fogo, eles foram cobertos por lã mineral resistente ao fogo. Os pilares de aço tinham 2.800 mm de altura e eram fixados à viga de base por meio de pinos de aço. Essas colunas foram feitas de aço Q235B e suas dimensões seccionais foram HN 200 mm × 200 mm × 8 mm × 12 mm. Os corpos de prova foram totalmente fixados às colunas de aço por meio de parafusos M22 de alta resistência ao atrito e placas de extremidade de aço que tinham dimensões de 210 mm × 160 mm × 10 mm (Figura 2(b)). A configuração de teste e o corpo de prova de viga mista pronto para teste são mostrados nas Figuras 2(c) e 2(d), respectivamente.



(uma)



(uma)

(b)

(c)

(d)

## Avanços em Ciência e Engenharia de Materiais

+ Journal Menu

PDF



Article Sections

A distribuição de temperatura e os deslocamentos da viga mista foram medidos durante os ensaios de incêndio. As temperaturas foram medidas em sete locais (A–C e E–H) dos corpos de prova. Especificamente, os termopares nas posições A–C e H monitoraram as temperaturas do concreto e vergalhões, enquanto os termopares nas posições E–G mediram as temperaturas do concreto e das vigas de aço. Para o concreto, os termopares foram dispostos com espaçamento de 20 mm na direção da espessura da laje. Além disso, as temperaturas foram medidas para as camadas superior e inferior de vergalhões, banzos superior e inferior de vigas de aço e alma de vigas de aço. Os detalhes da posição de medição são mostrados na Figura 3.

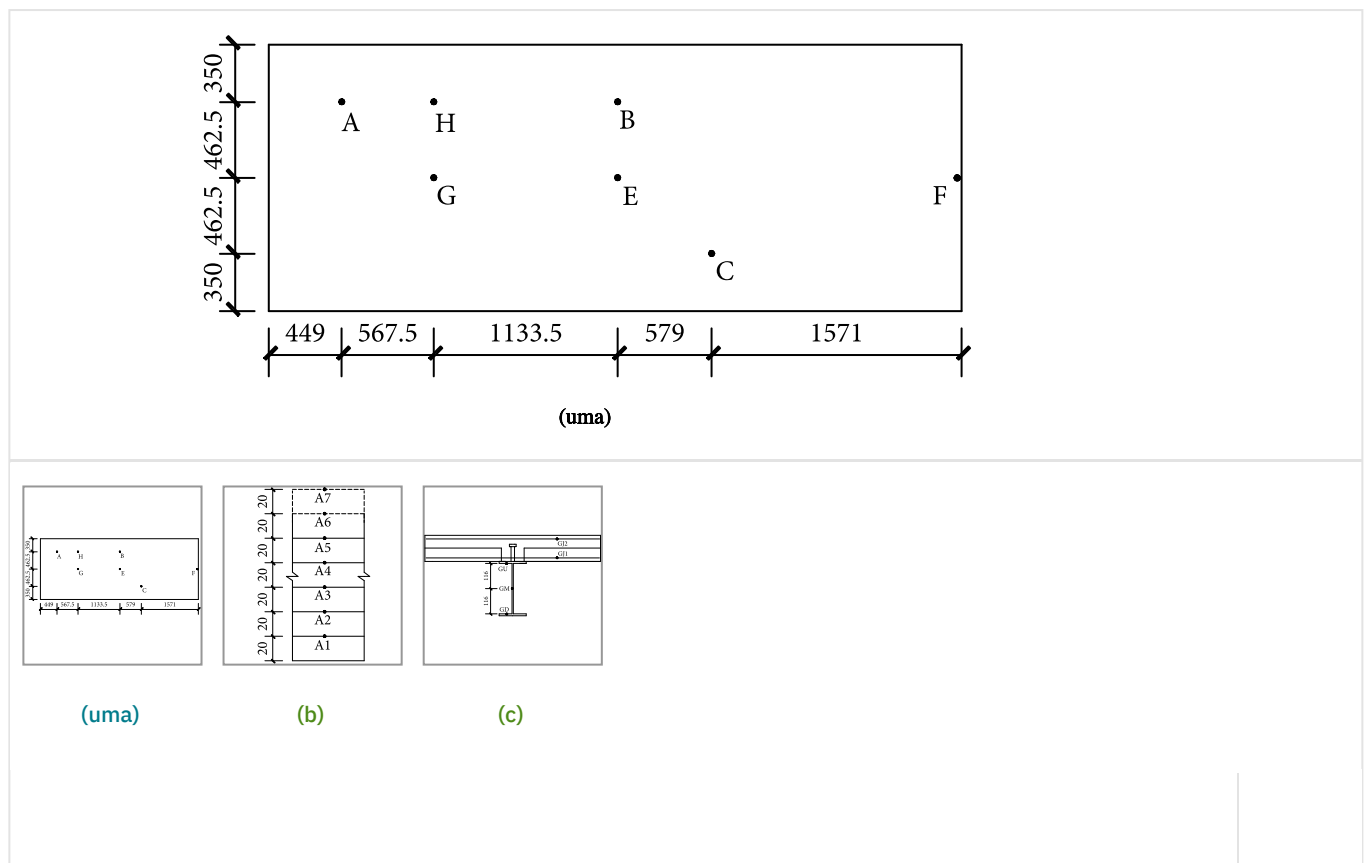


**Figura 3**

Temperature measurement positions: (a) plan arrangement, (b) measurement positions for concrete, and (c) measurement positions for rebars and steel beams.

The displacements of the composite beam specimens were measured using five linear variable differential transformers (LVDTs) arranged at selected positions (D1–D5) shown in Figure 4.

## Avanços em Ciência e Engenharia de Materiais

+ Journal Menu

PDF



Article Sections

### Figure 4

Arrangement of LVDTs.

### 2.5. Loading Scheme

In the test, two layers of iron blocks were placed on the top surface of the specimens to simulate a uniformly distributed load (UDL) of  $3.5 \text{ kN/m}^2$ . Figure 5 shows the layout of the iron blocks. After the UDL was applied, the specimens were heated according to the standard ISO-834 temperature curve.

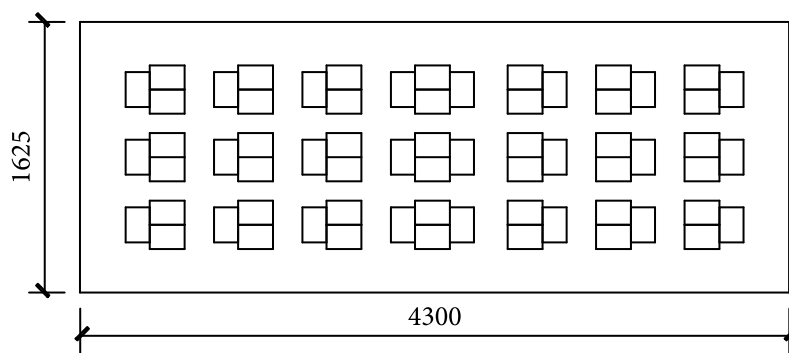


### Figure 5

Layout of the iron blocks.

## 3. Experimental Results and Discussion

### 3.1. Experimental Observations and Failure Modes

Two fire tests were carried out, in which the specimens SCB-1 and SCB-2 were tested at the same time and the specimen SCB-3 was tested separately. The main structural responses and failure modes of the three specimens are given below.

#### 3.1.1. SCB-1

After being heated for 8 minutes, a bursting sound occurred from the superposed slabs. At 10 minutes of the fire test, an overall vibration of the composite beam, accompanied by a loud sound, was observed. At

## Avanços em Ciência e Engenharia de Materiais

+ Journal Menu

PDF



☰ Article Sections



(a)



(a)



(b)



(c)

**Figure 6**

Failure modes of SCB-1: (a) water bay, (b) cracks on the top surface of the slab, and (c) local bursts on the bottom surface of the slab.

The tested specimen was passively cooled to a room temperature condition, during which no abnormal incident was observed. The main failure characteristics were as follows. (1) A large crack, as shown in Figure 6(b), on the top surface of SCB-1 extended from one end of the composite beam toward its midspan with gradually narrowed crack width. The maximum width of the crack was about 1 mm. (2) Vertical cracks were developed on the two longitudinal sides of the concrete slab and mainly concentrated above the superposing interface. Moreover, they were also observed in the postcast joint areas. (3) Vertical cracks appeared on the two transverse sides of the concrete slab and they were mainly distributed above the steel beam. (4) No cracks were observed on the bottom surface of the concrete slab yet local bursts happened (Figure 6(c)). (5) At the end restraints, the weld joint between the top flange of the steel beam and the steel column was torn, which might be the source of the loud sound during the test. An overall torsional deformation of the steel beam was also observed.

### 3.1.2. SCB-2

When the SCB-2 was heated for 13 minutes, the composite beam generated an overall vibration, accompanied by a loud sound. Another loud sound was made again at 25 minutes. Water spots (Figure 7

## Avanços em Ciência e Engenharia de Materiais

+ Journal Menu

PDF



☰ Article Sections



(a)



(a)

(b)

(c)

(d)

### Figure 7

Failure modes of SCB-2: (a) water spots, (b) severe out-of-plane instability of the slab, (c) cracks on the top surface of the slab, and (d) local bursts on the bottom surface of the slab.

Similar to the SCB-1, the failure modes of SCB-2 were examined after it was passively cooled to a room temperature condition. (1) The top surface cracks (Figure 7(c)) appeared from both ends of the slab and grew toward its midspan along the longitudinal direction. The same maximum crack width of 1 mm was also measured from the SCB-2 specimen. (2) Similar distribution patterns of the vertical cracks were developed on both longitudinal and transverse side surfaces of the concrete slab while local bursts (Figure 7(d)) also took place on its bottom surface. (3) In contrast with SCB-1, the weld joint for both top and bottom flanges of the steel beam fractured and produced the loud sound.

### 3.1.3. SCB-3

The overall specimen vibrations, together with loud sounds, occurred twice after 9 and 12 minutes of the fire test. At 18 minutes, a noticeable vertical deflection (Figure 8(a)) at the midspan of the specimen was observed. At 29 minutes, water spots were observed at both ends and midspan of the specimen, as shown in Figure 8(b). At 32 minutes, the out-of-plane buckling was generated in the tested specimen and increasingly aggravated, which ultimately stopped the test at 92 minutes.



## Avanços em Ciência e Engenharia de Materiais

+ Journal Menu

PDF



Article Sections

(a)



(a)

(b)

(c)

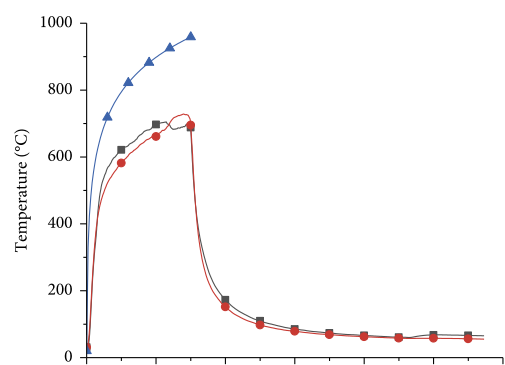
### Figure 8

Failure modes of SCB-3: (a) vertical deflection, (b) water spots, and (c) local bursts on the bottom surface of the slab.

Compared to the other two specimens, local concrete bursts (Figure 8(c)) also occurred on the bottom surface of the superposed slab, yet a relatively longer crack with a 1,205 mm length was produced on its top surface. Moreover, the weld joint for both top and bottom flanges fractured, which led to an overall distortion of the steel beam.

### 3.2. Temperature Field Analysis

The comparison of the actual furnace temperatures of the two tests and the ISO standard heating curve is shown in Figure 9(a), which shows that the trends of the furnace temperature change fairly followed the ISO standard. The rapid temperature rise also suggests that the fire flashover was well simulated. The nearly identical furnace temperature curves of the two tests indicate that a similar temperature distribution in the three specimens could be achieved. The test results of SCB-2 are given below and analysed to present a typical thermal response of composite beams with superposed slabs.



## Avanços em Ciência e Engenharia de Materiais

+ Journal Menu

PDF



☰ Article Sections

(a) (b) (c) (d)

### Figure 9

Temperature field analysis of SCB-2: (a) comparison of temperature curves, (b) temperature changes at position A, (c) temperature changes at position B, and (d) temperature changes of the steel beam.

As shown in Figures 9(b) and 9(c), owing to the thermal inertia of concrete, the temperature of the composite beam flange decreased along the height of the superposed slab section. The highest temperature was achieved at the bottom of the superposed slab, whereas the lowest one was found at its top. The most drastic change of the temperature along the slab cross section was found in the region with a distance of 40 mm to the slab bottom. With respect to the cooling, the temperature at the slab bottom went down faster than the ones at other regions in the same slab section. Due to the variation of the temperature distribution, a temperature gradient was produced along the thickness of the superposed slab. As a result, temperature stresses were generated within the slab and led to a tension effect in its top region. Such tensile temperature stresses, with the assistance of the bending moment due to the applied load, created top surface cracks along the longitudinal direction. Note that measurement position A in Figure 9(b) and position B in Figure 9(c) were at the superposed slab and the postcast joint, respectively. It is shown that the temperature gradients at these two positions were almost identical, which indicates that the superposing interfaces between the precast slabs and postcast top layers were not broken. In relation to the reinforcing bars, their temperatures were basically consistent with the surrounding concrete. The considerable temperature differences between the top (GJ2) and the bottom (GJ1) bars were mainly attributed to their distances to the source of the heat.

Figure 9(d) depicts the temperature changes measured at three positions on the midspan section of the steel beam. Specifically, EU and ED denote the measuring points on the top and bottom flanges, respectively, whereas EM denotes the measuring point on the web. The trends of three temperature changes were approximately the same and the maximum temperature of the steel beam was as high as 682°C. In the heating stage, the temperature of the top flange was lower than the other two positions as it was connected to the superposed concrete slab which absorbed a certain amount of the heat. In comparison, relatively less heat loss was caused on the web and the bottom flange of the steel beam as they were surrounded by hot air. In the cooling stage, the temperature of the bottom flange was lower than the ones of the other two positions. It is noted that the temperature of the concrete slab was higher than the one in the furnace due to its thermal inertia. Compared to the top flange and web, the bottom flange of the steel beam received less heat transfer.

The maximum temperatures of the steel beam and the concrete superposed slab were 682°C and 354°C, respectively. Such a large temperature difference led to incompatible deformations developed in the steel

## Avanços em Ciência e Engenharia de Materiais

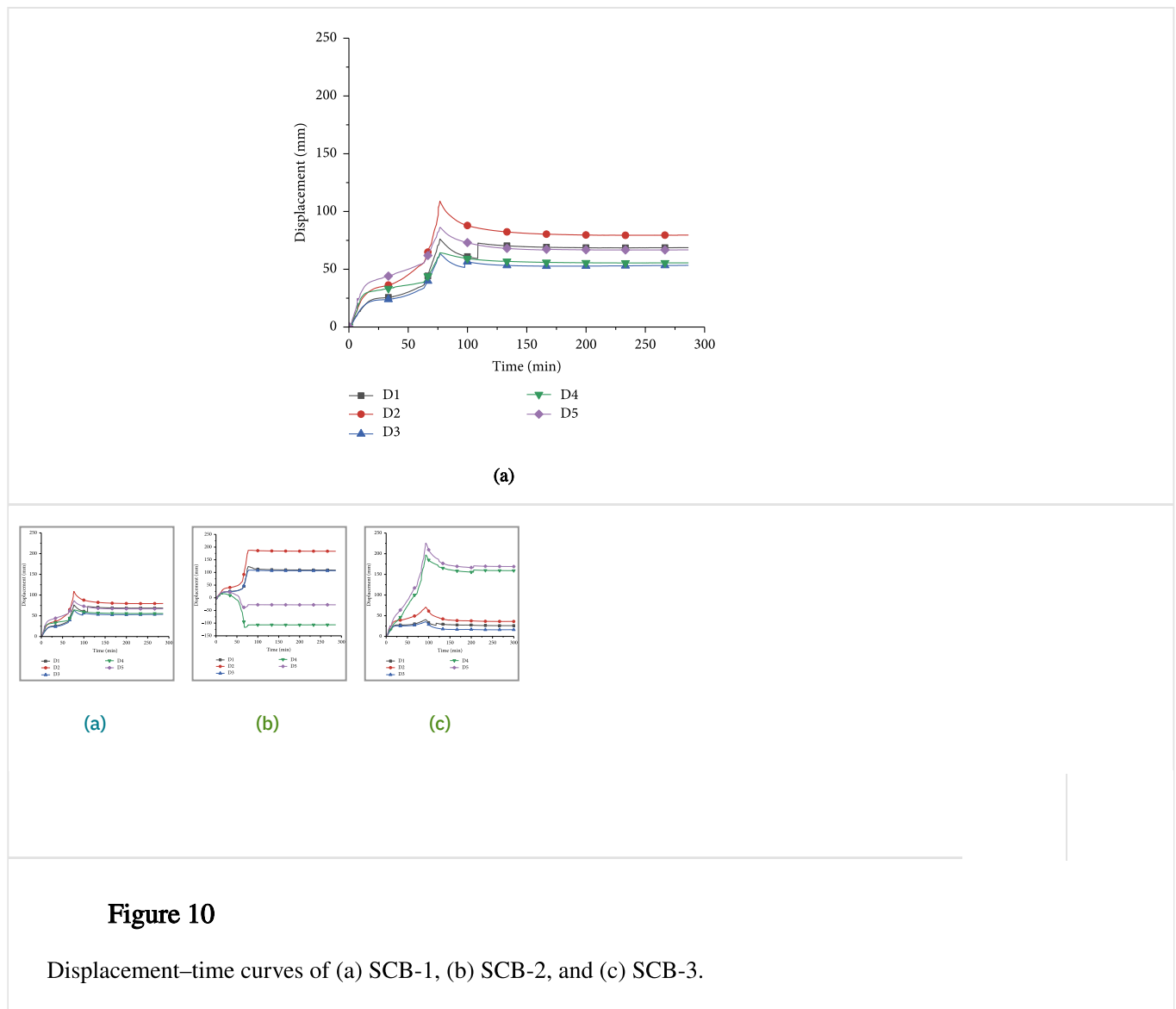
+ Journal Menu

PDF



### Article Sections

As shown in Figure 10, the displacement curves of SCB-1, SCB-2, and SCB-3 are presented. For SCB-1, as most of the gauges were on the upward movement side of the torsional axis, their displacement values were smaller than the ones of corresponding positions D1 and D2 which were approximately on the torsional axis. For SCB-2, due to a more severe torsional effect, the displacements at D4 and D5 shift from positive to negative, which indicates that their directions were changed from downward to upward during the test. In contrast to SCB-1 and SCB-2, D4 and D5 of SCB-3 were located on the downward movement side with respect to the torsional axis. As a result, larger displacement values were obtained when compared to D1 and D3.



The test data were collected until 287 minutes from the beginning of the SCB-1 test, in which a maximum displacement of 109.0 mm and a residual displacement of 79.6 mm were recorded, resulting in a deformation recovery ratio of 27.0%. The maximum displacement and the deformation recovery ratio of SCB-2 were not available due to its severe out-of-plane buckling failure. During the test period of 300

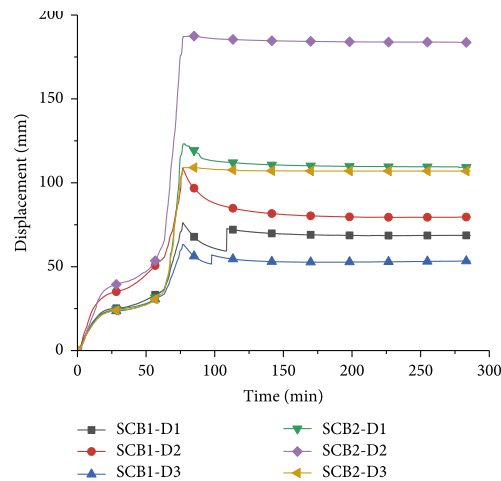
## Avanços em Ciência e Engenharia de Materiais

+ Journal Menu

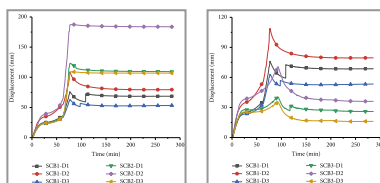
PDF



Article Sections



(a)



(a)

(b)

**Figure 11**

Comparisons of displacement developments of (a) SCB-1 and SCB-2 and (b) SCB-1 and SCB-3.

Figure 11(b) depicts the comparison of the displacement developments of SCB-1 and SCB-3. Although their displacement development patterns were also found to be similar in the heating stage, the two specimens behaved differently in the cooling stage. Moreover, the displacement values of SCB-1 were higher than the corresponding ones of SCB-3. It was largely because more shear studs with a smaller spacing were able to transfer more heat to the superposed slab, which further weakened its material and enlarged the overall deformation.

## 4. Numerical Simulation

Finite element models of the composite beams were created using a numerical analysis software ABAQUS. Sequenced thermomechanical coupling analysis was performed to simulate the fire tests and

## Avanços em Ciência e Engenharia de Materiais

+ Journal Menu

PDF



### Article Sections

The strengths, elastic moduli, and stress-strain relationships of concrete and steel at high temperature were determined according to the existing studies [17–21].

#### 4.2. Elements and Coupling Settings

Except for the reinforcement which was modelled using 2-node truss elements, all other components were created using 8-node solid elements.

In the temperature field simulation, the interactions between each part of the tested specimens were defined as “Ties” so that the heat can be transferred between different parts. In the thermomechanical coupling analysis, the reinforcing bars were “Embedded” into the concrete superposed slabs with other settings unchanged.

#### 4.3. Load and Boundary Conditions

The temperature field simulation was conducted firstly, after which the loads and boundary conditions were applied. The stresses of the model in the temperature field simulation were introduced as the initial stresses for the followed thermomechanical coupling analysis. The bottom ends of the steel columns were fully fixed and a UDL of  $3.5 \text{ kN/m}^2$  was applied to the top surfaces of the superposed slab models. The numerical model of a typical composite beam with superposed slabs specimen is shown in Figure 12.



**Figure 12**

Numerical model of the composite beam specimens.

# Avanços em Ciência e Engenharia de Materiais

+ Journal Menu

PDF



## Article Sections

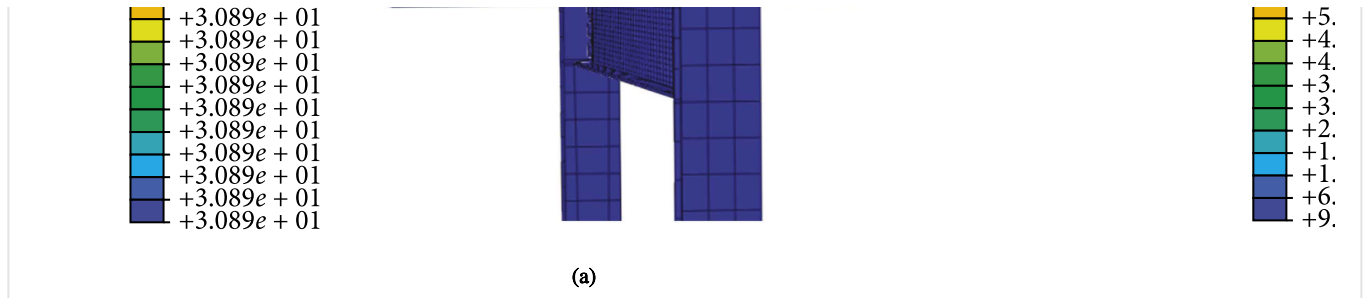
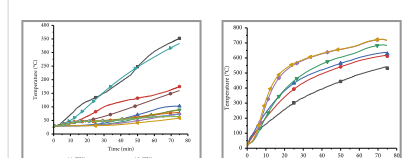
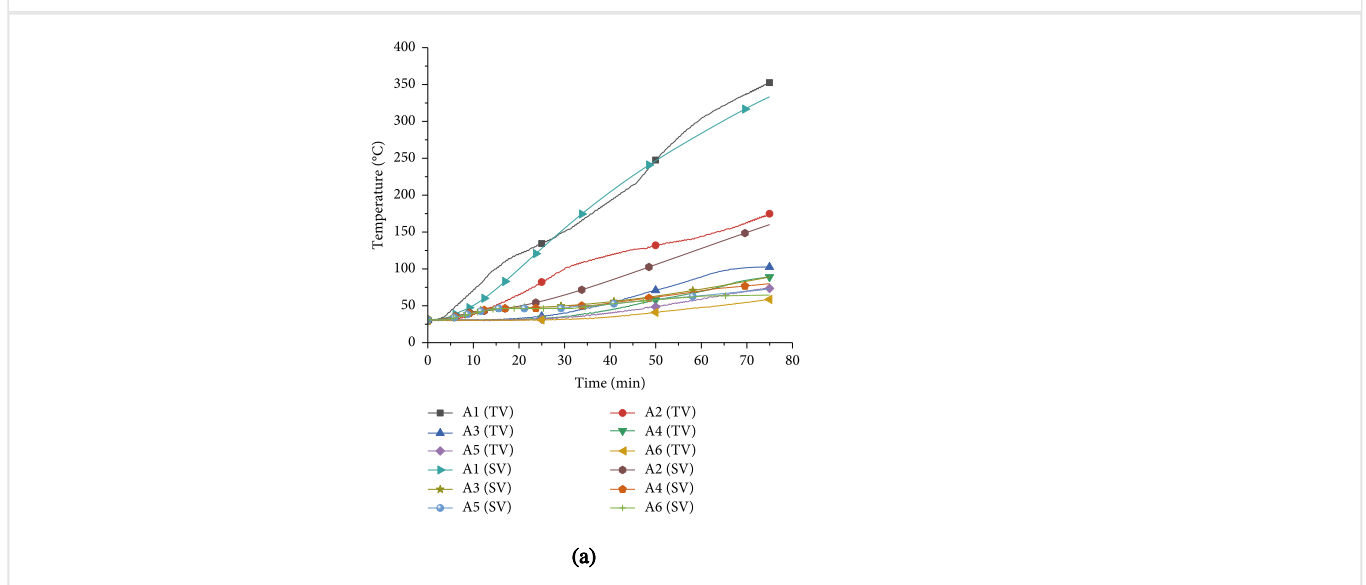


**Figure 13**

Temperature contours of SCB-2 (a) at 0 min and (b) at 75 min.



## Avanços em Ciência e Engenharia de Materiais

+ Journal Menu

PDF



### Article Sections

The displacement contours of the three tested specimens at the end of the heating stage are shown in Figure 15, while the simulated displacement developments at selected positions are compared against the corresponding test results in Figure 16. An accurate prediction of the overall displacement developments was achieved by the numerical models.

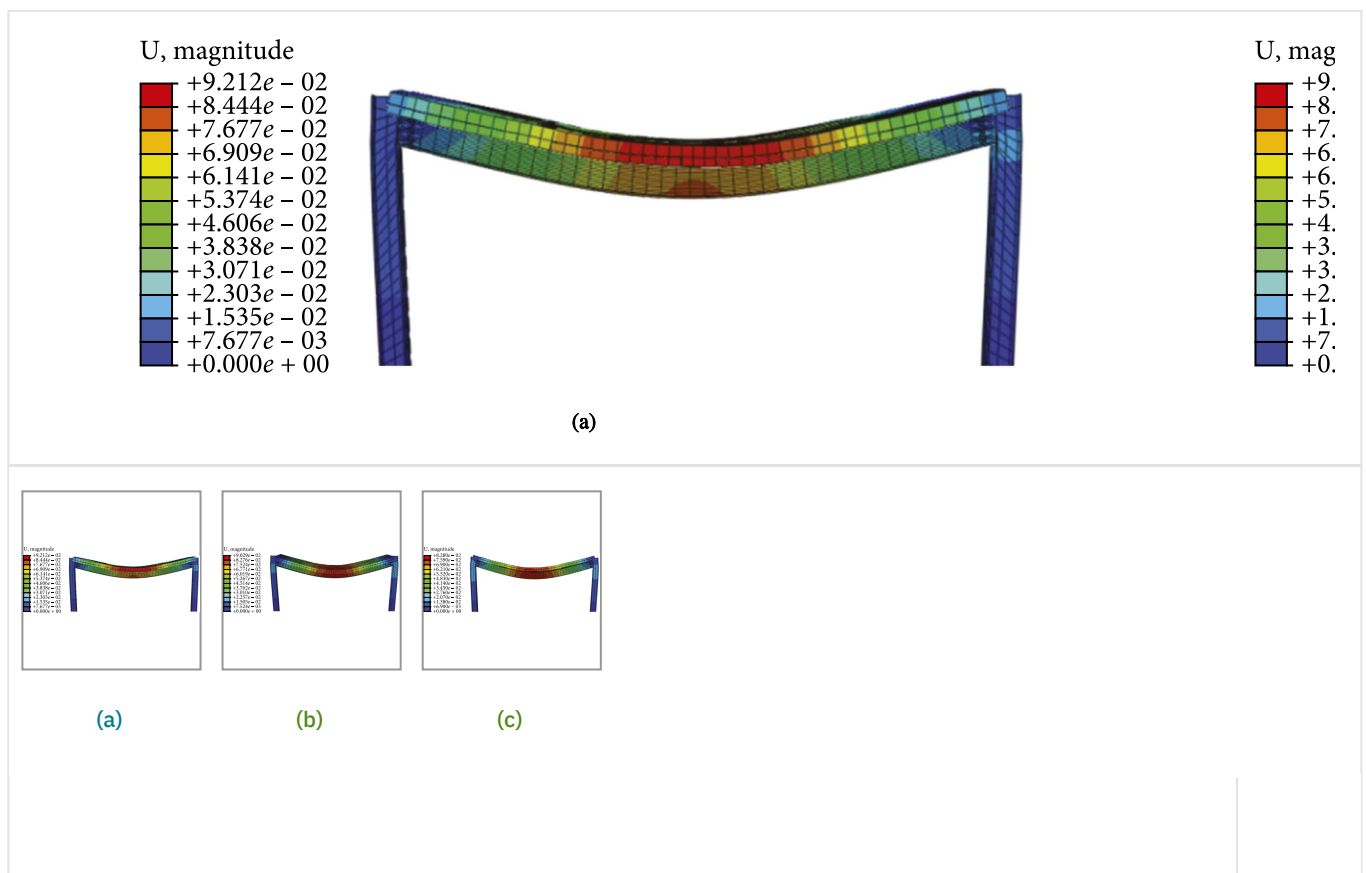


**Figure 15**

Displacement contours of three tested specimens: (a) SCB-1, (b) SCB-2, and SCB-3 (units are in m).



## Avanços em Ciência e Engenharia de Materiais

+ Journal Menu

PDF



☰ Article Sections

(a)

(b)

(c)

**Figure 16**

Comparison of displacement developments of three tested specimens: (a) SCB-1, (b) SCB-2, and (c) SCB-3.

## 5. Conclusion

To investigate the fire resistance of composite beams with restrained superposed slabs, three specimens were tested. Through further temperature field and displacement analyses and numerical simulations, the following conclusions were obtained.

- (1) In the heating stage, the temperature of the concrete superposed slabs decreased long their heights from the bottom. The most drastic change of the temperature along the slab cross section was the region with a distance of 40 mm to the slab bottom. The superposed concrete slabs could impose restraints to the steel beams due to their incompatible deformations.
- (2) Cracks were developed along the longitudinal direction on the top surfaces of the specimens due to the temperature stresses and the applied load. The superposing interfaces between the precast slabs and postcast top layers were not broken during the tests yet local bursts occurred on the bottom surfaces of the precast slabs.
- (3) The composite beams with restrained superposed slabs have an ability to recover a certain level of deformations after cooling.
- (4) With restraints, the spacing of shear studs could have a significant effect on the fire resistance of composite beams, especially for their deformation recovery capacities. In contrast, the effect of the thickness of the postcast top layers was negligible.
- (5) After simulating the temperature field and deformation behaviours of the specimens, the numerical results were found to agree well with the experiment data, which validated the developed numerical model.

## Data Availability

The data used to support the study findings are available from the corresponding author upon request.

## Conflicts of Interest



## Avanços em Ciência e Engenharia de Materiais

+ Journal Menu

PDF



### Article Sections

1. Lennon and D. Moore, "Client report: results and observations from full-scale fire test at BRE Cardington," Tech. Rep., Building Research Establishment, London, UK, 2004, Client report no. 215-741.  
View at: [Google Scholar](#)
2. B. R. Kirby, *The Behavior of a Multi-Storey Steel Framed Building Subjected to Fire Attack: Experimental Data*, British Steel, London, UK, 1998.
3. O. Mirza and B. Uy, "Behaviour of headed stud shear connectors for composite steel-concrete beams at elevated temperatures," *Journal of Constructional Steel Research*, vol. 65, no. 3, pp. 662–674, 2009.  
View at: [Publisher Site](#) | [Google Scholar](#)
4. J. H. Han, W. R. Cheng, Z. D. Xu et al., "Experimental study on the behaviors of profiled steel sheeting-concrete composite slabs on fire," *Industrial Construction*, vol. 36, no. 3, pp. 87–90, 2006, in Chinese.  
View at: [Google Scholar](#)
5. S. C. Jiang, G. Q. Li, G. B. Lou et al., "Numerical approach of behavior of steel-concrete composite slabs subjected to fire," *Journal of Building Structures*, vol. 25, no. 3, pp. 38–44, 2004, in Chinese.  
View at: [Google Scholar](#)
6. Z. H. Xu, Z. D. Lu, and L. G. Wang, "Nonlinear analysis of fire resistance of composite deck slabs," *Journal of Building Structures*, vol. 23, no. 5, pp. 73–83, 2002, in Chinese.  
View at: [Google Scholar](#)
7. S. G. Fan, Z. N. Li, H. Z. Wei et al., "Experimental study on membrane effect of steel deck concrete composite slabs on fire," *Journal of Disaster Prevention and Mitigation Engineering*, vol. 35, no. 1, pp. 44–50, 2015, in Chinese.  
View at: [Google Scholar](#)
8. Y. Z. Wang, *Behavior and Design of Composite Beam in Fire with Considering Global Structure Effect*, Tongji University, Shanghai, China, 2006.
9. H. Y. Zhou, G. Q. Li, and Y. Z. Wang, "Analysis of two factors influencing the fire resistance of composite beams," *Progress in Steel Building Structures*, vol. 8, no. 5, pp. 40–45, 2006, in Chinese.  
View at: [Google Scholar](#)

## Avanços em Ciência e Engenharia de Materiais

+ Journal Menu

PDF



### Article Sections

12. J. L. Lyu, Y. L. Dong, and Z. N. Yang, "Experimental and analytical studies on performance of edge beams of steel framed building subjected to fire," *Journal of Building Structures*, vol. 32, no. 9, pp. 92–98, 2011, in Chinese.  
View at: [Google Scholar](#)
13. J. L. Lyu, *Study on Fire Resistance of Beam and Column in the Overall Steel Frame*, Harbin Institute of Technology, Harbin, China, 2013.
14. China Architecture and Building Press, *Standard for Test Method of Mechanical Properties on Ordinary concrete:GB/T50081—200*, China Architecture and Building Press, Beijing, China, 2002.
15. Standards Press of China, *Materials—Tensile Testing—Part 1: Method of Test at Room Temperature: GB/T228. 1—2010*, Standards Press of China, Beijing, China, 2010.
16. T. T. Lie and E. M. A. Denham, "Factors affecting the fire resistance of circular hollow steel columns filled with bar-reinforced concrete," Tech. Rep., NRC-CNRC, Ottawa, Canada, 1993, NRC-CNRC internal report no. 651.  
View at: [Google Scholar](#)
17. Europe Committee for Standardization, *ENV1993-1-2, Eurocode 3, Design of Steel Structures, Part 1.2: Structures Fire Design*, Europe Committee for Standardization, Brussels, Belgium, 1993.
18. EN 1994-1-2, *Eurocode 4: Design of Composite Steel and Concrete Structures. Part 1-2: General Rules—Structural Fire Design*, British Standards Institution, London, UK, 2004.
19. Z. H. Guo and W. Li, *Summary of Experimental Research on Heat Resistance Mechanical Properties of Concrete*, Department of Civil Engineering, Tsinghua University, Beijing, China, 1991.
20. H. D. Li, *Experimental Research on Reinforced Concrete Compression-Bending Members under High Temperature*, Tsinghua University, Beijing, China, 1994.
21. China Architecture and Building Press, *Code for Design of Concrete Structures: GB 50010-2002*, China Architecture & Building Press, Beijing, China, 2002.

## Copyright

Copyright © 2020 Junli Lyu et al. This is an open access article distributed under the [Creative Commons Attribution License](#), which permits unrestricted use, distribution, and reproduction in any medium,

## Avanços em Ciência e Engenharia de Materiais

+ Journal Menu

PDF



### Article Sections

Chaowei Hao | Yanjiang Chen | ... | Laiyong Wang

reforçadas com chapas de aço

J. Branesh Robert | R. Angeline Prabhavathy | ... | Shubham Sharma

Comportamento de flexão de vigas de concreto armado com abertura circular na zona de flexão e zona de cisalhamento reforçadas com chapas de aço

Efeito de Enrijecedores Intermediários nos Comportamentos de Vigas de Aço Revestidas Parcialmente de Concreto

J. Branesh Robert | R. Angeline Prabhavathy | ... | Shubham Sharma

Cheng-Cheng Chen | Teguh Sudibyo

Follow us:



Sobre nós

Contate-Nos

Parcerias

Blogue

## Avanços em Ciência e Engenharia de Materiais

+ Journal Menu

PDF



 Article Sections

Corpus XML em hinduísta

Iniciativa de Arquivos Abertos

Prevenção de fraudes

---

[Política de Privacidade](#) | [Termos de Serviço](#) | [Política de Divulgação Responsável](#) | [Política de Cookies](#) | [Direitos autorais](#) | [Declaração da escravidão moderna](#)



## Avanços em Ciência e Engenharia de Materiais

+ Journal Menu

PDF



⋮ Article Sections

## Avanços em Ciência e Engenharia de Materiais

+ Journal Menu

PDF



☰ Article Sections



Baixe outros formatos



Encomende cópias impressas

